Automated 3D Lumbar Intervertebral Disc Segmentation from MRI Data Sets

Xiao Dong and Guoyan Zheng

Abstract This paper proposed an automated three-dimensional (3D) lumbar intervertebral disc (IVD) segmentation strategy from Magnetic Resonance Imaging (MRI) data. Starting from two user supplied landmarks, the geometrical parameters of all lumbar vertebral bodies and intervertebral discs are automatically extracted from a mid-sagittal slice using a graphical model based template matching approach. Based on the estimated two-dimensional (2D) geometrical parameters, a 3D variable-radius soft tube model of the lumbar spine column is built by model fitting to the 3D data volume. Taking the geometrical information from the 3D lumbar spine column as constraints and segmentation initialization, the disc segmentation is achieved by a multi-kernel diffeomorphic registration between a 3D template of the disc and the observed MRI data. Experiments on 15 patient data sets showed the robustness and the accuracy of the proposed algorithm.

1 Introduction

Intervertebral disc (IVD) degeneration is a major cause for chronic back pain and function incapacity [1]. Magnetic Resonance Imaging (MRI) has become one of the key investigative tools in clinical practice to image the spine with IVD degeneration not only because MRI is non invasive and does not use ionizing radiation, but more importantly because it offers good soft tissue contrast which allows visualization of the disc's internal structure [2].

MRI quantification has great potential as a tool for the diagnosis of disc pathology but before quantifying disc information, the IVDs need to be extracted

X. Dong (✉)
Faculty of Computer Science and Engineering, Southeast University, Nanjing, China
e-mail: xiao.dong@seu.edu.cn

G. Zheng
Institute for Surgical Technology and Biomechanics, Bern University, Bern, Switzerland
e-mail: guoyan.zheng@ieee.org

G. Zheng and S. Li (eds.), *Computational Radiology for Orthopaedic Interventions*, Lecture Notes in Computational Vision and Biomechanics 23, DOI 10.1007/978-3-319-23482-3_2

from the MRI data. IVD extraction from MRI data comprises two key steps. Firstly, all IVDs have to be detected from the images and secondly, the regions belonging to IVDs have to be segmented. Manual extraction methods [3, 4] as well as automated extraction methods [5–11] have been presented before. Since manual extraction is a tedious and time-consuming process which lacks repeatability, automated methods are preferred.

There are different approaches for automatizing the extraction of IVDs from medical images such as graphical model [5], probabilistic model [6], Random Forest regression and classification [12, 13], watershed algorithm [7], atlas registration [8], statistic shape model [10], graph cuts [9], and anisotropic oriented flux [11]. But stable and accurate IVD segmentation remains a challenge.

In this paper we propose an automated 3D lumbar IVD extraction method with minimal user interaction from MRI data sets. The main contribution of our method is a combination of graphical model-based spine column localization with a multi-kernel diffeomorphic registration-based segmentation. The motivation of the proposed strategy to first identify the spine column structure and then carry out the IVD segmentation stems from the following observation:

> The IVD geometries are highly constrained by the geometry of the spine column. If the geometrical parameters of the spine column and each individual vertebral body can be estimated accurately from the observed images, then they can provide both geometrical and appearance information about the intervertebral discs, which helps to improve the accuracy and robustness of the IVD segmentation.

The work flow of the proposed algorithm consists of the following three steps:

Initialization Two user supplied landmarks on a user selected mid-sagittal slice are required to indicate the centers of L1 and L5 vertebral bodies.

Lumbar spine column identification and modeling Starting from the user initialization, the 3D geometry of the lumbar spine column is automatically extracted from the 3D data sets, which is achieved as a sequential 2D + 3D model fitting procedure. The outputs of the lumbar spine column modeling procedure are the 3D geometric information of each individual vertebral body of L1–L5 and a *soft-tube* model that fits the outer surface of the lumbar spine column.

Lumbar disc segmentation The extracted lumbar spine column can provide reliable prior information for the initialization and constraints of the disc segmentation such as positions, sizes and image appearance of discs. The disc segmentation is finally achieved as a 3D multi-kernel diffeomorphic registration between a disc template and the observed data.

The paper is organized as follows. Section 2 describes details of the method, followed by experimental results in Sect. 3. Discussions and conclusions are presented in Sect. 4.

2 Methods

2.1 Data Sets

All datasets used in this paper were generated from a 1.5 T MRI scanner (Siemens medical solutions, Erlangen, Germany). Dixon protocol was used to reconstruct four aligned high-resolution 3D volumes during one data acquisition: in-phase, opposed-phase, water and fat images, as shown in Fig. 1. Each volume has a resolution of 2 mm × 1.25 mm × 1.25 mm and the data set size is 40 × 512 × 512. The advantage of working with such datasets is that different channels provide complementary information for our disc segmentation task. In our proposed segmentation strategy, we always first extract either intensity or feature information about different tissues on each of the 4 channels and then combine the 4 channel data into a single dataset as explained later.

2.2 Initialization

On the mid-sagittal slice, two landmarks are picked to indicate the centers of L1 and L5 vertebral bodies as shown in Fig. 2a.

2.3 Lumbar Spine Column Identification

Based on the initialization, we first carry out a 2D vertebral body and disc identification to localize vertebrae L1–L5 and the 5 target discs from the mid-sagittal slice. The geometrical information of the 2D identification is then used to guide a further 3D lumbar spine column modeling.

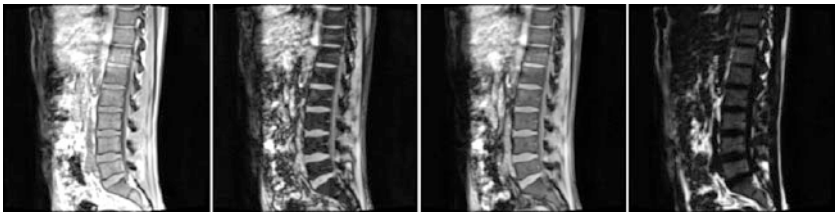

Fig. 1 The four aligned channels of a patient data, *left* to *right* in-phase, opposed-phase, water and fat images (for visualization purpose, we only show the middle sagittal (mid-sagittal) slice of each channel)

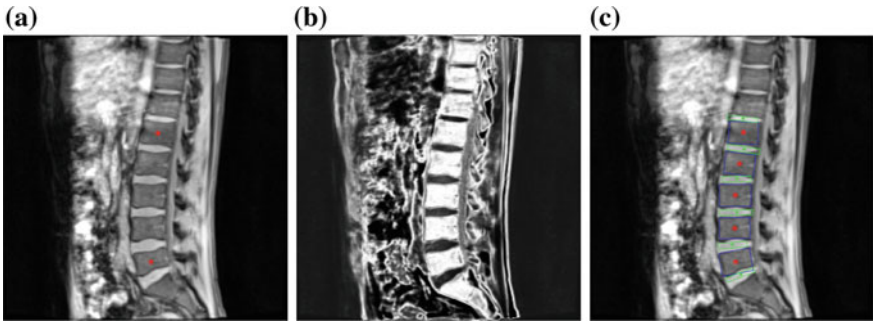

Fig. 2 Initialization and 2D lumbar spine column detection. **a** User initialization by picking *two landmarks* indicating the centers of L1 and L5 in the middle sagittal slice. **b** Probability assignment (displayed as *grey values*) of the bone tissue in the mid-sagittal slice for 2D lumbar spine column detection. **c** 2D lumbar spine column detection result using the graphical model based detection algorithm, *blue* and *green rectangles* representing the vertebral bodies and IVDs respectively (Color figure online)

2.3.1 2D Vertebral Body and Disc Identification

Solutions for spine location and disc labeling include feature-based bottom-up methods, statistical model-based methods and graphical model-based solutions. For a detailed review of the existing methods, we refer to [14, 15]. In this paper, the 2D vertebral body and disc identification is achieved using a graphical model based strategy introduced in [14]. Compared with the graphical models in [5, 6], the advantage of the graphical model in [14] is that both the low level image observation model and the high level vertebra context potentials need not to be learned from training data. Instead they are capable of self-learning from the image data during the inference procedure. The basic idea is to model both the vertebral bodies and discs in the mid-sagittal slice as parameterized rectangles, where the parameters are used to describe the geometries of these rectangles including their centers, orientations and sizes. The graphical model based spine column identification can be understood as matching the parameterized models with the observed images while also considering the geometrical constraints between neighboring vertebral bodies and discs. The exploration of geometrical constraints between vertebral components helps to enhance the identification robustness.

1. *The graphical model*: The graphical model used in this work to represent the lumbar spine column is given in Fig. 3. In this model each node V_i represents a connected disc-vertebra-disc chain of the spine column, whose geometrical parameters are given by X_i. On this graphical model we define
   - *The component observation model* $p(I|X_i)$ of a single component V_i representing the probability that the configuration X_i of the node V_i match the observed images I.

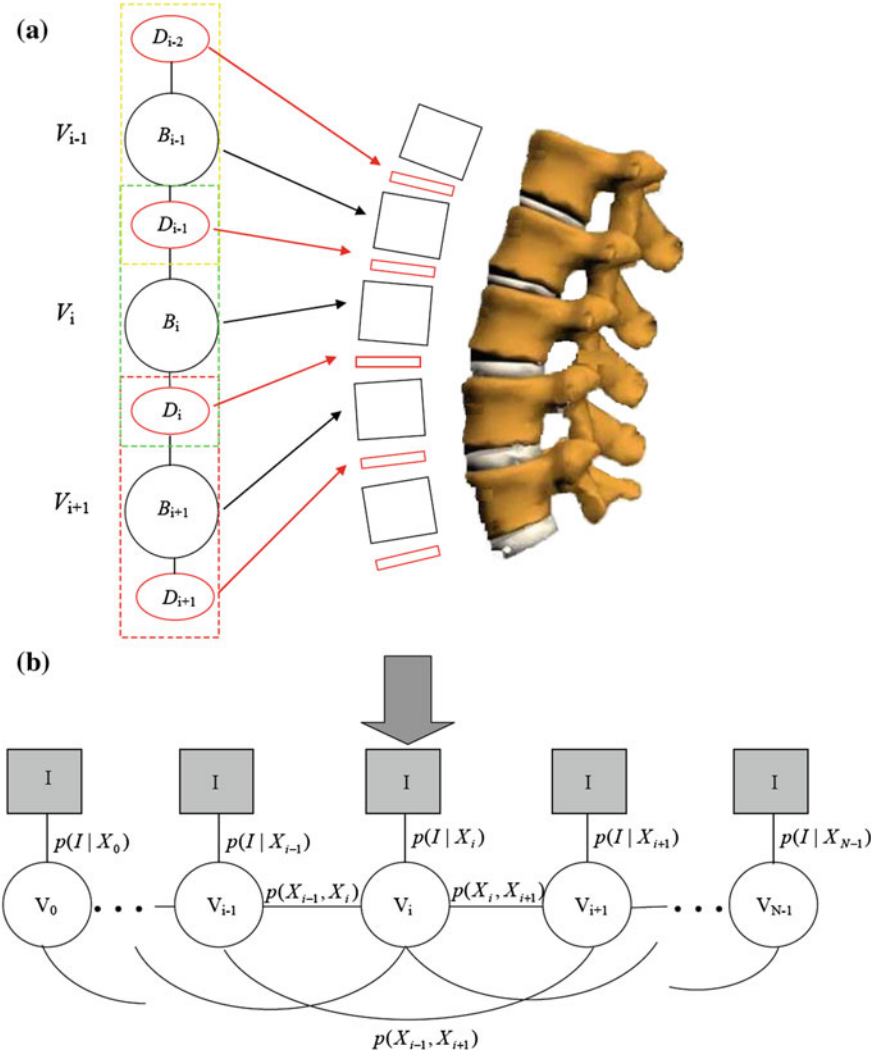

Fig. 3 Graphical model for the 2D lumbar spine column detection. **a** A node V_i represents a disc-vertebra − disc ($D_{i-1} - B_i - D_i$) chain of the lumbar spine and both the discs and vertebrae are modeled as parameterized *rectangles*. **b** The observation model $p(I|X_i)$ of each node V_i and potentials $p(X_i, X_j)$ between nodes V_i, V_j defined on the graphical model

- *The potentials $p(X_i, X_j)$ between neighboring components* V_i and V_j encoding the geometrical constraints between components which are defined by the anatomical structure of the spine column.

  The identification of the spine column from the mid-sagittal slice can then be formalized as to find the optimal configurations of $\{V_i\}$, $X = \{X_i\}$ that maximize

$$P(X|I) \propto \Pi_i p(I|X_i)\Pi_{i,j} p(X_i, X_j) \tag{1}$$

with

$$p(I|X_i) = p_I(I|X_i)p_G(I|X_i) \tag{2}$$

and

$$p(X_i, X_j) = p_S(X_i, X_j)p_O(X_i, X_j)p_D(X_i, X_j) \tag{3}$$

$p_I(I|X_i)$ and $p_G(I|X_i)$ stand for the probabilities that the observed image intensity and image gradient distributions match the geometrical parameters X_i respectively. $p_S(X_i, X_j)$, $p_O(X_i, X_j)$ and $p_D(X_i, X_j)$ are the geometrical constraints on the sizes, orientations and distances between neighboring components. All the observation models and constraints can be designed according to the observed data and prior anatomical knowledge of the spine structure. For detailed formulation of these terms, we refer to [14].

2. *Preprocessing of the 4 channel data*: In order to achieve the model fitting simultaneously on the 4 data channels, we need a preprocessing to combine the information from different data channel. As shown in the introduction of the graphical model, in the component observation model $p(I|X_i)$, both the image intensity and gradient information are used by $p_I(I|X_i)$ and $p_G(I|X_i)$ respectively. In order to combine the information of the 4 channels, we firstly observe that besides the positions of L1 and L5, the two user selected landmarks and the mid-sagittal slice also provide intensity distribution information of the bony tissue in the 4 channel volumes. For the intensity information, by fitting a Gaussian distribution $N(\mu_i, \sigma_i)$, $i = 1, 2, 3, 4$ to a small neighbourhood of the initialization landmarks on each data channel, we can estimate the intensity distribution of the bone region of that data channel and accordingly assign to each pixel at position (l, k) with intensity value $x_i^{(l,k)}$ of the mid-sagittal slice a value $p_i^{l,k} = \frac{1}{\sqrt{2\sigma_i^2}} \exp(\frac{-(x_i^{(k,l)} - \mu_i)^2}{2\sigma_i^2})$ indicating the probability that the pixel belongs to the vertebral body. The combined bone assignment probability information of the 4 channels can then easily be obtained by an equally weighted averaging of the 4 channels as $p^{k,l} = \frac{1}{4}\sum_i p_i^{l,k}$. Similarly we can also combine the gradient information of the 4 data channels by simply averaging the gradient amplitude of each channel. The combined intensity and gradient information are then used in the intensity and gradient local observation model components, $p_I(I|X_i)$ and $p_G(I|X_i)$, of the graphical model. Figure 2b shows an example of the bone tissue probability assignment on the mid-sagittal slice computed from the user supplied 2 landmarks (Figs. 2a and 4 channel volume data (see Fig. 1 for an example).

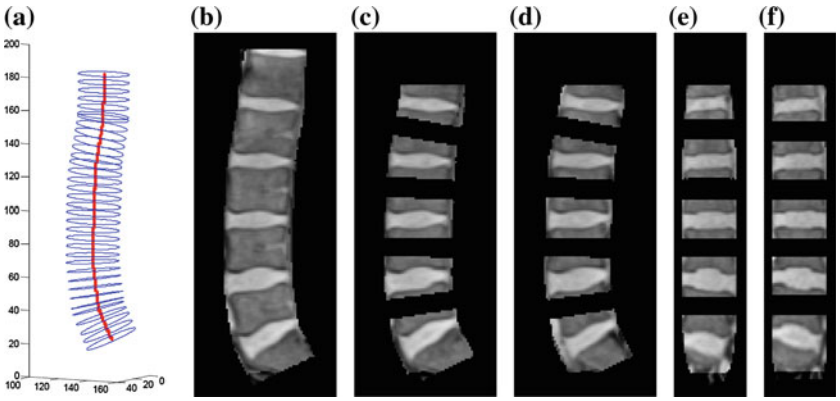

Fig. 4 3D lumbar spine column detection and modeling. **a** The 3D soft-tube model of the lumbar spine column; **b** segmented lumbar spine column image; **c**–**d** segmented disc candidate regions in sagittal slices; **e**–**f** segmented disc candidate regions in coronal slices. Although all tasks are conducted in 3D, here we show the results in 2D slices for visualization purpose

3. *Optimization*: The optimization is achieved as an inference on the graphical model, which is essentially a particle based nonparametric belief propagation on the graphical model as described in Algorithm 1. The outputs are then the 2D geometrical parameters of the spine column which best fit the observed mid-sagittal slices of all the 4 data channels.
4. *Detection results*: Fig. 2c gives the 2D lumbar column detection result. It can be observed that the centers, sizes and orientations of the vertebral bodies and IVDs are correctly identified.

Algorithm 1 Graphical model based inference for 2D lumbar spine column detection

Input: Bone region assignment map (Fig. 2b) from mid-sagittal slices of the 4 data channel, landmarks from user initialization
Output: 2D geometrical parameters of the lumbar vertebral bodies ($L_1 - L_5$) and discs between $L_1 - S_1$
Initialization: Roughly estimate the possible configuration regions of the positions, sizes and orientations of each vertebral body and disc according to the user initialization and prior anatomical information of the lumbar spine.
Start: $t = 0$, draw N random samples configurations of $\{X_i^n(t), n = 1, \ldots, N\}$ of each model node V_i from the estimated parameter space.
while not converge **do**

1. Compute the *belief* of each particle $X_i^n(t)$ by the local observation model as $b_i^n(t) \propto p(I|X_i^n(t))$.
2. Run belief propagation till converge on the chain graphical model using the potentials $p(X_i^n, X_j^{n'})$ among nodes to update the *belief* of each particle $X_i^n(t)$ to obtain updated *believes* $\{\bar{b}_i^n(t)\}$, which are the approximations of the marginal probabilities $P(X_i^n|I)$ given in (1) obtained by the belief propagation.
3. Re-sample the particles according to the updated believes $\{\bar{b}_i^n(t)\}$ to obtain new samples $\bar{X}_i^n(t)$ of each node.

(continued)

(continued)

Algorithm 1 Graphical model based inference for 2D lumbar spine column detection

4. Update the configuration of each sample $\bar{X}_i^n(t)$ by a Gaussian random perturbation on the parameters to obtain new particles $\{X_i^n(t+1)\}$.
5. $t = t + 1$.

end while
For each node V_i, the parameters of the particle with the highest belief are selected as the configuration of that node and therefore the geometrical parameters of the vertebral bodies and discs are estimated.

2.3.2 3D Lumbar Spine Column Modeling

The above explained 2D lumbar spine column model only provides an incomplete information of the spine column. Therefore, in order to accurately localize the lumbar column and the geometrical parameters of each vertebral body and disc, a 3D lumbar spine model is needed. To achieve this, we model each lumbar vertebral body as an elliptical cylinder and the lumbar spine column as a variable-radius soft tube. Details of the modeling procedure are described as follows:

- 3D modeling of each vertebral body
  (a) If we approximately model the vertebral body as a cylinder, then from the 2D vertebral body identification results, the position, hight, radius and orientation of each vertebral body and the image intensity distribution of the bone region in each data channel (also modeled as a Gaussian distribution) can be estimated.
  (b) Given the estimated bone tissue intensity distribution of each data channel, then for each voxel in the neighbourhood of the estimated cylinder model of the vertebra body, we can assign the probability if this voxel belongs to the bone tissue. We can also integrate the information of 4 channels in the same way as explained in the 2D model fitting procedure to obtain the combined bone tissue probability assignment $p^{k,l,m}$ for a voxel at position (k, l, m).
  (c) From the bone tissue probability assignment of voxels around each vertebral body, we can further refine the 3D modeling of the vertebral bodies. To achieve this, we further model the vertebral body as an elliptical cylinder. Then a least-squares geometric fitting to the voxels which are assigned with a high enough probability ($p^{k,l,m} > 0.8$) of belonging to the bone tissue can extract the 3D geometry of each vertebral body, including the center, height, orientation and the major radius and minor radius of the elliptical cylinder model.

- *3D modeling of the spine column* Given the 3D model of each vertebral body, we can further construct the 3D lumbar column model. We model the lumbar column as a variable-radius soft tube that best fits the outer surfaces of all the extracted vertebral bodies. Given the 3D models of L1–L5 vertebral bodies, the central axis and the variable-radius of the soft tube can be obtained by a linear interpolation on the centers and radii of the extracted 3D models of vertebral bodies. This results of this 3D variable-radius soft-tube spine column model is shown in Fig. 4a.

Obviously given the 3D soft-tube lumbar spine column model, the spine column region can be extracted from the observed data sets (Fig. 4b). By further eliminating the bony tissue region using the 3D models of vertebral bodies, the candidate region for each target disc can be localized as shown in Fig. 4c–f. The following 3D IVD segmentation is then carried out on the extracted candidate IVD regions.

2.4 3D Disc Segmentation

We solve the 3D disc segmentation as a template based registration between a geometrical disc template and the observed data.

- The IVD template is set as a thin elliptical cylinder. Considering the anatomical structure of the spine column, i.e., each IVD must fall between its neighbouring vertebral bodies, the initial geometries (center, radii, orientation, hight) of the IVD cylinder template can be estimated using the 3D spine column model and the geometries of its neighboring vertebral bodies, which are all available from the previous 3D lumbar spine column modeling procedure.
- For the segmentation of a specific IVD, the correspondent observed data to be matched is just the extracted candidate IVD region as shown in Fig. 4c–f.
- For the registration algorithm we choose the multi-kernel diffeomorphic image matching in the Large Deformation Diffeomorphic Metric Mapping (LDDMM) framework as described in [16] and related literatures [17–20].

2.4.1 Multi-kernel LDDMM Registration

LDDMM framework [19] is one of the two main computational frameworks in computational anatomy [17]. Existing works show that LDDMM is a general solution for nonrigid image registration with a high flexibility and accuracy. In [16, 18, 21] multi-scale LDDMM registration algorithms were investigated. Compared with the LDDMM registration with a single kernel, multi-kernel LDDMM has the capability to optimize the deformation in multiple spatial scales [16].

Following the general idea of LDDMM framework, we formalize the multi-kernel image registration between two images I_0 and I_1 as an optimization problem to find the optimal time dependent velocity field $v(t)$ that minimizes a cost function $\mathcal{E}(\{v^k(t)\})$ as the sum of a deformation energy term and an image similarity term formalized as

$$\mathcal{E}(\{v^i(t)\}) = \frac{1}{2}\sum_i^K w^i \int_0^1 \|v^i(t)\|_{V^i}^2 dt + \|I_0 \circ \phi_v^{-1}(1) - I_1\|_{L^2}^2 \tag{4a}$$

$$\frac{\partial}{\partial t}\phi_v(t) = v(t) \circ \phi_v(t) \tag{4b}$$

$$v(t) = \sum_i^K v^i(t) \tag{4c}$$

$$\phi_v(0) = Id \tag{4d}$$

where $\|v^i(t)\|_{V^i} = \langle v^i(t), v^i(t)\rangle_{V^i}^{\frac{1}{2}}$ is the norm induced by the inner product $\langle u, v\rangle_{V^i} = \langle L_{V^i}u, L_{V^i}v\rangle_{L^2}$ defined on the ith scale. $\{K_{V^i} = (L_{V^i}^+ L_{V^i})^{-1}\}, i = 1, \ldots, K$ are the K kernels which essentially are used to encode the image deformation energy at different spatial scales and w^i is the weighting factor of the deformation energy of the ith kernel. $\phi_v(t)$ is the time-dependent deformation computed as the integration of the velocity field $v(t)$ and $I_0 \cdot \phi_v^{-1}(t)$ is the transformed image of I_0 by the deformation $\phi_v(t)$.

Using the optimal control based approach introduced in [22, 23], we get the Euler-Poincare equation (EPDiff) (5a)–(5f) of the optimal velocity fields $\{v^k(t)\}$, k = 1, 2, …, K for the multi-kernel LDDMM registration algorithm.

$$\dot{I}(t) = -\nabla I(t) \cdot v(t) \tag{5a}$$

$$\dot{P}(t) = -\nabla(P(t) \cdot v(t)) \tag{5b}$$

$$v(t) = \sum_{k=1}^K v^k(t) \tag{5c}$$

$$v^k(t) = -(w^k)^{-1} K_{V^k} \star (P(t)\nabla I(t)), \quad k = 1, \ldots, K \tag{5d}$$

$$P(1) = -(I(1) - I_1) \tag{5e}$$

$$I(0) = I_0 \tag{5f}$$

The registration algorithm is given as follows:

For more details on the computation routine and the performance of the multi-kernel LDDMM registration algorithm, we refer to [19, 22, 23].

2.4.2 Disc Segmentation by Diffeomorphic Registration

The IVD segmentation is achieved as a template based registration between the thin cylinder IVD template and the correspondent candidate disc region as shown in Fig. 4.

In order to explore both intensity and feature information to enhance the accuracy and robustness of the segmentation, we consider a simultaneous registration of two pairs of images, I_0^I/I_1^I and I_0^E/I_1^E, which stand for the image intensity and edge information template/observation pairs respectively. Accordingly in the cost function of the LDDMM registration (4a), the image similarity term includes two components $\|I_0^I \circ \phi_v^{-1}(1) - I_1^I\|_{L^2}^2 + \beta\|I_0^E \circ \phi_v^{-1}(1) - I_1^E\|_{L^2}^2$ with I_0^I/I_1^I and I_0^E/I_1^E as explained below.

Algorithm 2 Multi-Kernel LDDMM registration

Input: Images to be registered I_0, I_1
Output: Time dependent velocity field $v(t)$, $t \in [0, 1]$ whose integration gives the optimal matching process $I(t)$, $t \in [0, 1]$ which represents a smooth deformation from I_0 to I_1.
Initialization: $I(0) = I_0$, $v^k(t) = 0$, $t \in [0, 1]$, $k = 1, 2, \ldots, K$
while not converge **do**

1. Compute $I(t)$, $t \in [0, 1]$ by (5a), (5b), (5f).
2. Compute $P(1)$ by (5e).
3. Update $P(t)$, $t \in [0, 1]$ by solving (5c) in the inverse direction.
4. Update $v^i(t)$, $t \in [0, 1]$, $i = 1, 2, \ldots, K$ by (5d).

end while

Intensity information The template intensity image I_0^I is just the initialized disc template, i.e., a binary 3D image with the interior region of the disc template set as 1. The correspondent target image I_1^I is constructed by a three-step procedure.

1. Based on the 3D spine column model, for each vertebra disc, we can determine a region that belongs to the interior region of the disc with high confidence as explained in Fig. 5.
2. From the extracted high confidence disc voxels, we can estimate the image intensity distribution of the disc tissue in each data set by assuming a Gaussian intensity distribution $N(u_i, \sigma_i)$, $i = 1, 2, 3, 4$, i.e., to estimate the values $\{u_i, \sigma_i\}$, $i = 1, 2, 3, 4$ for each channel volume.
3. Accordingly in each channel volume I_i^{MRI}, $i = 1, 2, 3, 4$, each voxel $v_i^j \in I_i^{MRI}$ in the candidate disc region with an intensity value I_i^j can be assigned a probability

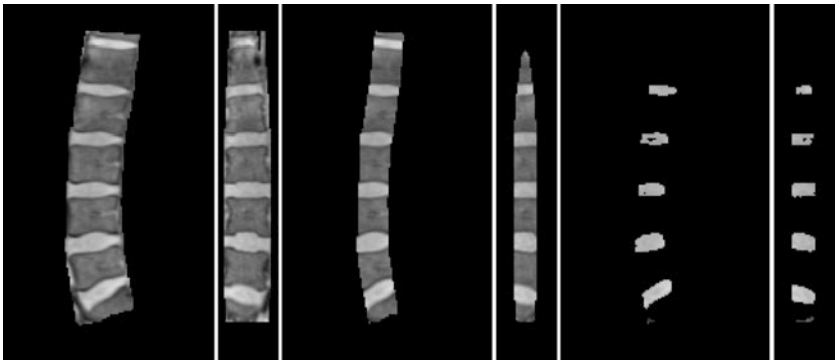

Fig. 5 Determination of the high confidence disc region using the spine column model. *Left* to *right* The spine column region extracted using the spine column model shown in a sagittal and a coronal slice; The central region of the spine column obtained by shrinking the radius of the spine column model by a factor 0.5 shown in the same two slices; The detected high confidence disc regions by further cutting out the bone tissue using the spine column model

$p_i^j = \frac{1}{\sqrt{2\pi\sigma_i^2}} \exp(-\frac{(I_i^j - u_i)^2}{2\sigma_i^2})$ indicating whether voxel v_i^j belongs to the disc region using the correspondent Gaussian distribution model $N(u_i, \sigma_i)$, $i = 1, 2, 3, 4$. The image I_1^I that contains the intensity information of the 4 channel data is then constructed as an average of the probabilities of the 4 data sets $\{P_i = \{p_i^j\}, v_i^j \in I_i^{MRI}, i = 1, 2, 3, 4\}$ as $I_1^I = (\prod P_i)^{\frac{1}{4}}$. Figure 6c–f show an example of the intensity template and the computed correspondent target image.

Edge information For the edge information, the template image I_0^E can be regarded as the outer surface of the disc template as shown in Fig. 6g–h. The target image I_1^E can be obtained by summing up and normalizing the gradient amplitudes of the 4 data set, see Fig. 6i–j.

An example of the template images and the correspondent target images and the time dependent registration procedure is shown in Fig. 6.

By registering the disc template to the observed 3D data volume, the final segmented IVD can then be obtained as the deformed template achieved by the multi-kernel LDDMM registration.

3 Experiments

The proposed algorithms are verified on MRI datasets of 15 patients obtained with the Dixon protocol. In all the data sets, based on the two landmarks obtained from the initialization step, both the 2D lumbar spine column and the 3D spine column

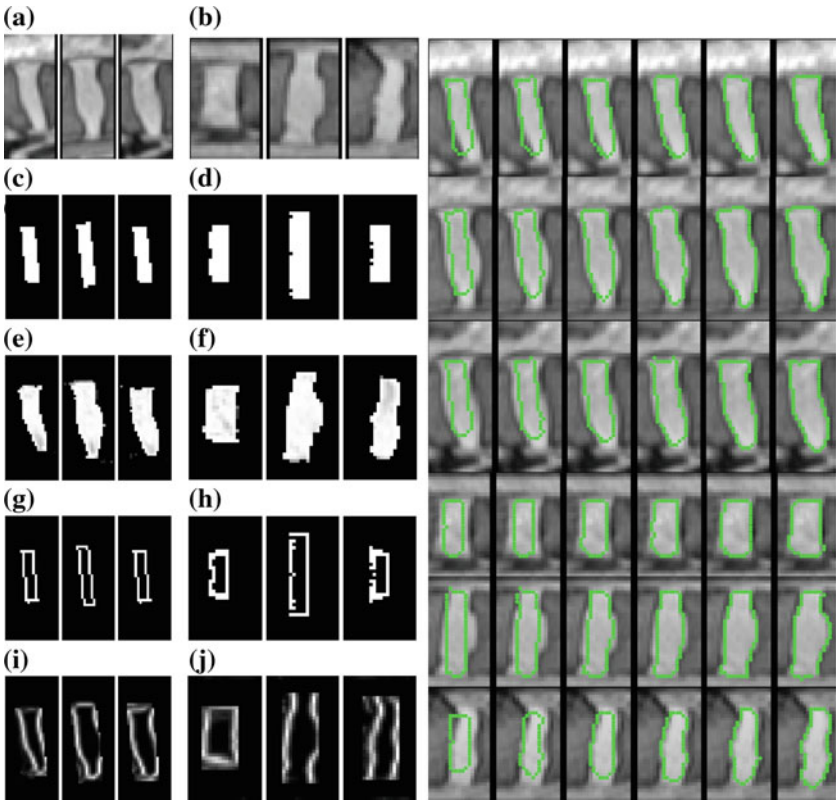

Fig. 6 3D IVD segmentation by multi-kernel LDDMM registration. *Left side* the data used in diffeomorphic registration based 3D lumbar disc segmentation. Although the task was performed in 3D, we show results on 2D slices for visualization purpose. Also be aware that in the target images, the bone tissue regions are extracted using the spine column model. **a**, **b** 3 sagittal/coronal slices of the candidate disc region (disc L4–L5 in Fig. 2) **c**, **d** the intensity disc template in 3 sagittal/coronal slices; **e**, **f** intensity information extracted from MRI data sets in 3 sagittal/coronal slices; **g**, **h** the edge disc template in 3 sagittal/coronal slices; **i**, **j** edge information computed from MRI data sets in 3 sagittal/coronal slices; *Right side* the time-dependent deformation of the disc template during the multi-kernel diffeomorphic registration for a L4–L5 disc segmentation. *Left* to *right* the deformations of the template at 6 time slots t = 0, 0.2, 0.4, 0.6, 0.8, 1. t = 0 means the initial template and t = 1 gives the final registration results; from *top row* to *bottom row*: the evolution of the template visualized in 6 different slices

models are correctly extracted. The computational time of each data set varies between 10–15 min depending on the initialization and converge speed with a MATLAB implementation. Examples of the disc segmentation results on 4 patient data sets are shown in Fig. 7.

We also carried out quantitative evaluation of our algorithm. To do this, we manually segmented all datasets (we only need to segment one channel for each

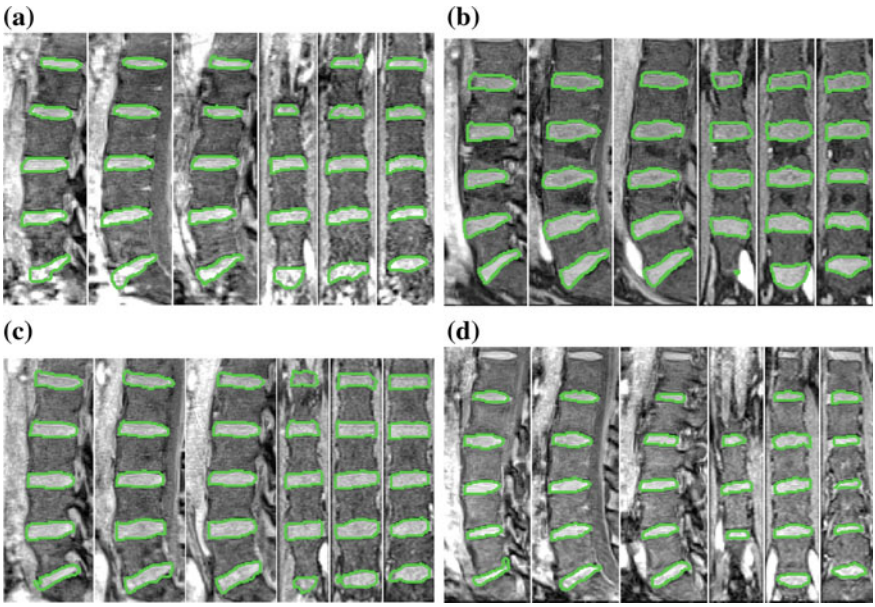

Fig. 7 3D intervertebral disc segmentation results on 4 patients. For visualization purpose, we display the results on 2D slices. For each image, the *left* three columns are sagittal slices and the *right* three are coronal slices

patient as all four channel volumes are aligned according to Dixon imaging protocol) and took the binary volumes from the manual segmentation as the ground truth to verify the accuracy of the present algorithm. We computed the Dice coefficient D which is usually used to measure the overlap between two binary images:

$$D = \frac{2 \times |A \cap B|}{|A| + |B|} \times 100 \tag{6}$$

Table 1 shows the average dice coefficients of the 5 discs on all 15 patients when the automated segmentation was compared to the manual segmentation. The highest average dice coefficient was found for patient #8 (87.9 %) and the lowest average dice coefficient was found for patient #9 (80.5 %). We also computed the average dice coefficients for all discs and the results are presented in Table 2. We note that Neubert et al. [10] reported a mean Dice of 76–80 % in their 3D IVD segmentation paper.

Table 1 Average dice coefficients (%) of the 5 discs between the manual segmentation and the proposed algorithm on different patients

Patient	P1	P2	P3	P4	P5	P6	P7	P8	P9	P10	P11	P12	P13	P14	P15
Dice	86.1	81.9	82.6	86.3	86.8	83.6	87.6	87.9	80.5	84.1	86.3	85.4	86.9	87.7	83.1

Table 2 Average dice coefficients (%) between the manual segmentation and the proposed algorithm on different discs on all 15 data sets

Disc	L1–L2	L2–L3	L3–L4	L4–L5	L5–S1
Dice	81.2	87.1	88.2	86.5	82.7

4 Conclusions

In this paper we proposed an automated lumbar intervertebral disc segmentation strategy, whose key components include a graphical model based spine column identification algorithm and a multi-kernel LDDMM registration algorithm to achieve the disc segmentation. By identifying the lumbar spine column structure before carrying out the segmentation, we acquire geometrical and appearance information about the spine column. These information can be used to accurately locate the candidate disc region and provide constraints to enhance the performance of the disc segmentation. By converting the segmentation problem as a template based diffeomorphic registration, we can explore both the intensity and edge information of the observed data while keeping a smooth deformation of the template so that the final segmented discs will possess smooth surfaces. The experiments on 15 patient data sets verified the robustness and accuracy of our method. We also noticed that for abnormal cases, such as with missing/additional vertebrae or the scoliosis case, the automated lumbar column identification may not be reliable although the graphical model can handle the unknown vertebra number as shown in [14]. A possible solution for these extreme cases is to ask the user to indicate the center of each vertebra body during the initialization step. Once the centers are known, the particle filtering based inference can still achieve a reliable 2D lumbar column identification and the following up 3D lumbar column modeling and disc segmentation.

References

1. Modic M, Ross J (2007) Lumbar degenerative disk disease. Radiology 1:43–61
2. Parizel P, Goethem JV, den Hauwe LV, Voormolen M (2007) Degenerative disc disease. In Van Goethem J (ed) Spinal imaging—diagnostic imaging of the spine and spinal cord. Springer, Berlin, pp 122–133
3. Tsai M, Jou J, Hsieh M (2002) A new method for lumbar herniated intervertebral disc diagnosis based on image analysis of transverse sections. Comput Med Imaging Graph 26:369–380
4. Niemelainen R, Videman T, Dhillon S, Battie M (2008) Quantitative measurement of intervertebral disc signal using MRI. Clin Radiol 63:252–255
5. Schmidt S, Kappes JH, Bergtholdt M, Pekar V, Dries S, Bystrov D, Schnorr C (2007) Spine detection and labeling using a parts-based graphical model. In: Karssemeijer N, BL (ed) IPMI 2007. Springer, Berlin, pp 122–133

6. Corso J, Alomari R, Chaudhary V (2008) Lumbar disc localization and labeling with a probabilistic model on both pixel and object features. In: Metaxas D (ed) MICCAI 2008. Springer, Berlin, pp 202–210
7. Chevrefils C, Cheriet F, Aubin C, Grimard G (2009) Texture analysis for automatic segmentation of intervertebral disks of scoliotic spines from MR images. IEEE Trans Inf Technol Biomed 13:608–620
8. Michopoulou S, Costaridou L, Panagiotopoulos E, Speller R, Panayiotakis G, Todd-Pokropek A (2009) Atlas-based segmentation of degenerated lumbar intervertebral discs from MR images of the spine. IEEE Trans Biomed Eng 56:2225–2231
9. Ayed IB, Punithakumar K, Garvin G, Romano W, Li S (2011) Graph cuts with invariant object-interaction priors: application to intervertebral disc segmentation. In: Szekely G, HH (ed) IPMI 2011. Springer, Berlin, pp 221–232
10. Neubert A, Fripp J, Schwarz R, Lauer L, Salvado O, Crozier S (2012) Automated detection, 3d segmentation and analysis of high resolution spine MR images using statistical shape models. Phys Med Biol 57:8357–8376
11. Law M, Tay K, Leung A, Garvin G, Li S (2013) Intervertebral disc segmentation in MR images using anisotropic oriented flux. Med Image Anal 17:43–61
12. Glocker B, Feulner J, Criminisi A, Haynor D, Konukoglu E (2012) Automatic localization and identification of vertebrae in arbitrary field-of-view CT scans. In Ayache N (ed) MICCAI 2012. Springer, Berlin, pp 590–598
13. Glocker B, Zikic D, Konukoglu E, Haynor D, Criminisi A (2013) Vertebrae localization in pathological spine CT via dense classification from sparse annotations. In Mori K (ed) MICCAI 2013. Springer, Berlin, pp 262–270
14. Dong X, Lu H, Sakurai Y, Yamagata H, Zheng G, Reyes M (2010) Automated intervertebral disc detection from low resolution, sparse MRI images for the planning of scan geometries. In: Wang F, Yan P, Suzuki K, Shen D (eds) MLMI2010. Springer, Berlin, pp 10–17
15. Dong X, Zheng G (2015) Automated 3D lumbar intervertebral disc segmentation from MRI data sets. In: Yao J, Glocker B, Klinder T, Li S (eds) Recent advances in computational methods and clinical applications for spine imaging. Lecture notes in computational vision and biomechanics, vol 20. Springer, Berlin, pp 131–142
16. Risser L, Vialard FX, Wolz R, Murgasova M, Holm DD, Rueckert D (2011) Simultaneous multiscale registration using large deformation diffeomorphic metric mapping. IEEE Trans Med Imaging 30:1746–1759
17. Grenander U, Miller MI (1998) Computational anatomy: an emerging discipline. Q Appl Math 4:617–694
18. Sommer S, Nielsen M, Lauze F, Pennec X (2011) A multi-scale kernel bundle for LDDMM: towards sparse deformation description across space and scales. In: Szekely G, HH (ed) IPMI2011. Springer, Berlin, pp 624–635
19. Beg MF, Miller MI, Trouv A, Younes L (2005) Computing large deformation metric mappings via geodesic flow of diffeomorphisms. Int J Comput Vision 61:139–157
20. Miller MI, Trouv A, Younes L (2006) Geodesic shooting for computational anatomy. J Math Imaging Vision 24:209–228
21. Bruveris M, Gay-Balmaz F, Holm DD, Ratiu TS (2011) The momentum map representation of images. J Nonlinear Sci 21:115–150
22. Hart GL, Zach C, Niethammer M (2009) An optimal control approach for deformable registration. In: CVPR2009, pp 9–16
23. Vialard FX, Risser L, Rueckert D, Cotter CJ (2012) Diffeomorphic 3d image registration via geodesic shooting using an efficient adjoint calculation. Int J Comput Vision 97:229–241

http://www.springer.com/978-3-319-23481-6

Computational Radiology for Orthopaedic Interventions
Zheng, G.; Li, S. (Eds.)
2016, VIII, 376 p. 200 illus., Hardcover
ISBN: 978-3-319-23481-6